

Investigation of Thermo-Hydraulic Performance for Different Arrangements of Ribs in Rectangular Solar Air Channel



J. Singh, A. Sharma, and R. Chauhan

Nomenclature

D	Diameter (m)
d	Discrete distance from outer edge of the rib (m)
d/x	Relative gap position (dimensionless)
e	Thickness of rib (m)
e/D _h	Relative roughness height (dimensionless)
f	Friction factor (dimensionless)
g	Discrete width (m)
g/e	Relative gap width (dimensionless)
H	Height of the channel (m)
Nu	Nusselt number (dimensionless)
P	Pitch of the ribs (m)
P/e	Relative roughness pitch (dimensionless)
Re	Reynolds number (dimensionless)
W	Width of the channel (m)
W/w	Relative roughness width (dimensionless)
W/H	Duct aspect ratio (dimensionless)
w	Width of the ribs (m)
x	Half length of the rib

J. Singh · A. Sharma (✉) · R. Chauhan
Department of Mechanical Engineering, Dr B R Ambedkar National Institute of Technology,
Jalandhar, Punjab 144011, India
e-mail: ashutoshs.me.19@nitj.ac.in

Greek Symbols

α	Angle of attack (dimensionless)
$\alpha/90$	Relative angle of attack (dimensionless)

Subscripts

ar	Arc ribs
dar	Discrete arc ribs
dmar	Discrete
dVr	Discrete V-shape ribs
dmVr	Discrete multiple V-shape ribs
H	Hydraulic
Mar	Multiple arc ribs
mVr	Multiple V-shape ribs
S	Smooth surface
Vr	V-shape ribs

1 Introduction

The effective utilization is very much necessary for energy converting machine in order to achieve maximization in desired form of energy yield. Solar air channels are generally used for heating the air by utilizing solar energy. In solar air channel, the air passes beneath an absorber plate which receives energy from the solar radiations [1]. Then heat energy is transferred to air which is further used for different applications. The effectiveness of solar air channel is quite low due to very poor convective heat transfer between the air and heated plate, i.e., absorber plate of solar air channel [2]. Its thermal performance can be increased by inducing different turbulent geometries within the air flow channel which separates the laminar sublayer on the absorber plate [3]. However, modifications in flow channel with intention to increase thermal performance also offer significant amount of hurdles to air flow. So while designing the turbulent geometries both of these parameters, i.e., thermal and hydraulic performance should be taken into consideration. For increasing the performance of solar air channel, various shapes and types of geometries have been studied in the literature. Most of these turbulent geometries are in the form of ribs [4–11], baffles, fins, protrusions, dimples, etc. [12]. Generally, these different studies had carried out to identify the thermal and hydraulic performance individually at different flow conditions. For identifying the overall performance of any roughness geometry, effect of both thermal and hydraulic performance should be considered concurrently and at same flow conditions. Thermo-hydraulic performance parameter

(THPP) accounts together the hydraulic and thermal performance of the roughness geometry simultaneously under same flow conditions. In the present study, different arrangements of ribs as roughness geometry have considered for estimating thermal, hydraulic, and thermo-hydraulic performance. These parameters have been evaluated for different flow conditions, i.e., Reynolds number. Correlations provided in literature for Nusselt number (Nu) and friction factor (f) for different geometries have been used to estimate performance parameters.

2 Rib Roughness Geometries

Various geometries of ribs as roughness over the absorber plate of solar air channel have been studied in literature. In this study, rib geometries in arc and V-shape have been selected because of their effective performance. The selected geometries have been presented in this section.

2.1 Arc Ribs

The influence of arc ribs made from circular wire, in air flow channel of solar air channel was studied by Saini and Saini [4]. The schematic of the geometry with potential parameters is shown in Table 1. These parameters were varied in a definite range and optimum values were found out on the ground of performance. These parameters along with optimum values have been presented in Table 2. An enhancement of 3.8 and 1.75 was found for Nu and f , respectively from smooth channel. Based on the variation in performance with parameters, correlations that were developed for Nu_{ar} and f_{ar} , are presented in Table 1.

2.2 Discrete Arc Ribs

Hans et al. [5] investigated the effect of discrete arc ribs in solar air channel. Schematic of the discrete arc ribs and potential parameters has been presented in Tables 1 and 2, respectively. Developed correlations for Nu_{dar} and f_{dar} are also presented in Table 1. Authors observed that maximum increment in Nu_{dar} and f_{dar} was 2.63 and 2.44, respectively.

Table 1 Schematics and correlations for Nu and f of different geometries in solar air channel

Sr. no.	Geometry	Schematic	Correlations
1	Arc ribs		$Nu_{dar} = 0.001047Re^{1.3186}(e/D_h)^{0.3772}(\alpha/90)^{-0.1198}$ $f_{ar} = 0.14408Re^{-0.17105}(e/D_h)^{0.1765}(\alpha/90)^{0.1185}$
2	Discrete arc ribs		$Nu_{dmar} = 1.014 \times 10^{-3} Re^{1.036}(P/e)^{2.522}(\alpha/90)^{-0.293}(d/x)^{-0.078} \times (g/e)^{-0.016} \times (e/D_h)^{0.412}$ $\times \exp(-0.567(Ln(P/e))^2) \times \exp(-0.114(Ln(\alpha/90))^2) \times \exp(-0.077(Ln(d/x))^2) \times \exp(-0.133(Ln(g/e))^{2.0527})$ $f_{dar} = 8.1921 \times 10^{-2} (Re)^{-0.147} (P/e)^{1.191} (\alpha/90)^{-0.292} (d/x)^{-0.067} \times (g/e)^{-0.006} (e/D_h)^{0.528} \exp(-0.255(\ln(P/e))^2) \exp(-0.110(\ln(\alpha/90))^2)$ $\times \exp(-0.063(\ln(d/x))^2) \exp(-0.158(g/e)^2)$
3	Multiple arc ribs		$Nu_{mmar} = 1.564 \times 10^{-4} Re^{1.343}(e/D)^{0.048}(W/w)^{0.407} \times \exp(-0.099(Ln(W/w))^2)(P/e)^{0.572}$ $\times \exp(-0.148(Ln(P/e))^2) \times (\alpha/90)^{-0.355} \times \exp(-0.272(Ln(\alpha/90))^2)$ $f_{mar} = 0.063 \times (e/D)^{0.102} \times Re^{-0.16} \times (W/w)^{0.277} \times (p/e)^{0.562} \times (\alpha/90)^{0.023}$ $\times \exp(-0.140(Ln(p/e))^2) \times \exp(-0.013(Ln(\alpha/90))^2)$
4	Discrete multiple arc ribs		$Nu_{dmmar} = 1.39 \times 10^{-4} \times Re^{1.3701} \times (d/x)^{-0.4997} \times (g/e)^{-0.0292} \times (W/w)^{0.4017} \times (p/e)^{0.5854} \times (\alpha/60)^{-2.235} \times (e/D)^{0.0931}$ $\times \exp(-0.3989(Ln(d/x))^2) \times \exp(-0.2013(Ln(g/e))^2) \times \exp(-0.129(Ln(W/w))^2) \times \exp(-0.5614(Ln(\alpha/60))^2)$ $f_{dmar} = 2.11 \times 10^{-1} \times Re^{-0.25} \times (d/x)^{-0.888} \times (g/e)^{-0.079} \times (W/w)^{0.032} \times (p/e)^{0.643} \times (\alpha/60)^{-2.546} \times (e/D)^{0.145} \times \exp(-0.662(Ln(d/x))^2)$ $\times \exp(-0.496(Ln(g/e))^2) \times \exp(-0.160(Ln(p/e))^2) \times \exp(-3.96(Ln(\alpha/90))^2)$

(continued)

Table 1 (continued)

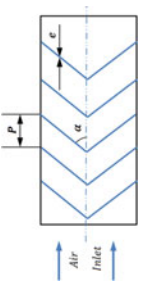
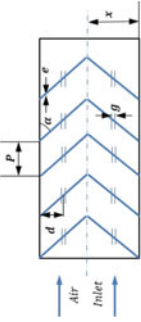
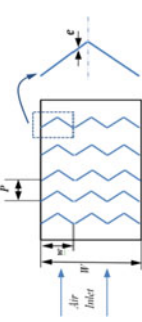
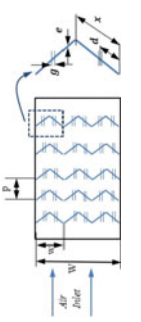
Sr. no.	Geometry	Schematic	Correlations
5	V-shape ribs		$Nu_{D,r} = 0.067 \times Re^{0.888} (\epsilon/D_h)^{0.424} (\alpha/60)^{-0.077} \times \exp[-0.782 \times (\ln(\alpha/60))^2]$ $f_{D,r} = 6.266 \times Re^{-0.425} \times (\epsilon/D_h)^{0.365} \times (\alpha/60)^{-0.093} \times \exp(-0.719 \ln(\alpha/60))^2$
6	Discrete V-shape ribs		$Nu_{D,r} = 2.36 \times 10^{-3} Re^{0.9} (P/\epsilon)^{3.5} (\alpha/60)^{-0.23} (d/x)^{-0.043} \times (g/\epsilon)^{-0.014} \times (\epsilon/D_h)^{0.47}$ $\times \exp(-0.84 \ln(P/\epsilon)^2) \times \exp(-0.72 \ln(\alpha/60))^2 \times \exp(-0.05 \ln(d/x))^2 \times \exp(-0.15 \ln(g/\epsilon)^{2.0852})$ $f_{D,r} = 4.13 \times 10^{-2} Re^{-0.126} \times (P/\epsilon)^{2.74} \times (\alpha/60)^{-0.034} \times (d/x)^{-0.058} \times (g/\epsilon)^{0.031} \times (\epsilon/D_h)^{0.70}$ $\times \exp(-0.685 \ln(P/\epsilon)^2) \times \exp(-0.93 \ln(\alpha/60))^2 \times \exp(-0.058 \ln(d/x))^2 \times \exp(-0.21 \ln(g/\epsilon)^{2.0852})$
7	Multiple V-shape ribs		$Nu_{D,m,r} = 3.35 \times 10^{-5} Re^{0.92} (\epsilon/D)^{0.177} (W/w)^{0.43} (\alpha/90)^{-0.49}$ $\times \exp(-0.117 \ln(W/w)^2) \times \exp(-0.61 \ln(\alpha/90))^2 (P/\epsilon)^{8.54} \times \exp(-2.0407 \ln(P/\epsilon)^2)$ $f_{D,m,r} = 4.47 \times 10^{-4} Re^{-0.3188} \times (\epsilon/D)^{0.73} \times (W/w)^{0.22} \times (\alpha/90)^{-0.39}$ $\times \exp(-0.52 \ln(\alpha/90)^2) \times (P/\epsilon)^{8.9} \exp(-2.133 \ln(P/\epsilon)^2)$
8	Discrete multiple V-shape ribs		$Nu_{D,m,r} = 8.532 \times 10^{-3} \times Re^{0.932} \times (\epsilon/D)^{0.175} \times (W/w)^{0.506} \times \exp(-0.0753 \ln(W/w)^2) (d/x)^{-0.03348}$ $\times \exp(-0.0653 \ln(d/x)^2) (g/\epsilon)^{-0.0708} \times \exp(-0.223 \ln(g/\epsilon)^2) (\alpha/60)^{-0.0239}$ $\times \exp(0.1153 \ln(\alpha/60)^2) (P/\epsilon)^{1.196} \times \exp(-0.2805 \ln(P/\epsilon)^2)$ $f_{D,m,r} = 3.19 \times Re^{-0.3151} \times (\epsilon/D)^{0.268} \times (W/w)^{0.1132} \times \exp(-0.0974 \ln(W/w)^2) (d/x)^{0.0610}$ $\times \exp(-0.1065 \ln(d/x)^2) (g/\epsilon)^{-0.1769} \times \exp(-0.6349 \ln(g/\epsilon)^2) (\alpha/60)^{0.1553}$ $\times \exp(-0.1527 \ln(\alpha/60)^2) (P/\epsilon)^{-0.7941} \times \exp(0.1486 \ln(P/\epsilon)^2)$

Table 2 Potential parameters of different arrangements of ribs as turbulent geometry

Sr. no.	Arrangements of ribs	Potential parameter	Re	e/d	$\alpha/90$	P/e	d/x	W/w	g/e	W/H
1	Arc ribs	Range	2000–17,000	0.0213–0.0422	0.333–0.666	10	–	–	–	12
		Optimum	–	0.0422	0.333	–	–	–	–	–
2	Discrete arc ribs	Range	2000–16,000	0.022–0.043	0.1666–0.8333	4–12	0.2–0.8	–	0.5–2.5	–
		Optimum	–	0.043	0.333	10	0.65	–	1	–
3	Multiple arc ribs	Range	2200–22,300	0.018–0.045	0.1666–0.8333	4–16	–	1–7	–	11
		Optimum	22,300	0.045	0.6667	8	–	5	–	–
4	Discrete multiple arc ribs	Range	2100–21,000	0.016–0.044	0.1666–0.8333	4–16	0.25–0.85	1–7	0.5–2.0	10
		Optimum	21,000	0.044	0.6667	8	0.65	5	1	–
5	V-shape ribs	Range	2500–18,000	0.02–0.034	0.333–1	10	–	–	–	10.15
		Optimum	–	0.034	0.6667	–	–	–	–	–
6	Discrete V-shape ribs	Range	3000–15,000	0.015–0.043	0.1666–0.8333	4–12	0.2–0.8	–	0.5–2.0	–
		Optimum	–	0.043	0.6667	8	0.65	–	1	–
7	Multiple V-shape ribs	Range	2000–20,000	0.019–0.043	0.1666–0.8333	6–12	–	1–10	–	–
		Optimum	–	0.043	0.6667	8	–	6	–	–
8	Discrete multiple V-shape ribs	Range	2000–20,000	0.022–0.043	0.1666–0.8333	6–12	0.24–0.80	1–10	0.5–1.5	10
		Optimum	–	0.043	0.6667	8	0.69	6	1	–

2.3 Multiple Arc Ribs

Effect of multiple arc ribs inside the solar air channel was observed by Singh et al. [6]. Schematic of the roughened absorber plate with potential parameters and developed correlations of Nu_{mar} and f_{mar} are shown in Table 1. Range of the potential parameters studied and optimum value found is depicted in Table 2. Maximum enhancement in Nu_{mar} and f_{mar} was founded as 5.07 and 3.71, respectively.

2.4 Discrete Multiple Arc Ribs

In continuation to the study of arc shapes in solar air flow channel, discrete multiple arc ribs were studied by Pandey et al. [7]. Schematics of the geometry and range of potential parameters is presented in Tables 1 and 2, respectively. The enhancement in Nu_{dmar} and f_{dmar} was founded 5.85 and 4.96, respectively.

2.5 V-shape Ribs

The study of ribs made of circular wire in V-shape was carried out by Momin et al. [8]. V-shape upstream ribs were studied for performance enhancement from smooth duct and it was found that Nu_{Vr} and f_{Vr} increases by 2.3 and 2.83 respectively. Schematic of the geometry used and correlations of Nu_{Vr} and f_{Vr} are presented in Table 1. The ranges of geometrical parameters with founded optimum values are shown in Table 2.

2.6 Discrete V-shape Ribs

Singh et al. [9] carried out research to investigate the effect of discrete V-shape ribs onto the performance of solar air channel. Top view of the plate used for experimentations is shown in Table 1. Potential parameters of the geometry with their range and founded optimum values have been presented in Table 2. From this study, it was concluded that Nu_{dVr} and f_{dVr} upsurges by 3.04 and 3.11, respectively.

2.7 Multiple V-shape Ribs

Variation in heat transfer rate and flow friction by introducing multiple V-shape ribs in rectangular air channel was studied by Hans et al. [10]. Table 1 depicts the schematic

of roughness geometry onto the absorber plate and ranges of potential parameters are presented in Table 2. By using the multiple V-shape ribs of optimum value, authors found maximum enhancement in Nu_{mVr} and f_{mVr} of 6 and 5, respectively, from smooth plate air channel. Correlations for Nu_{mVr} and f_{mVr} were also developed with an error of $\pm 10\%$ and are presented in Table 1.

2.8 Discrete Multiple V-shape Ribs

Extending the research on V-shape ribs, discrete multiple V-shape ribs were studied by Kumar et al. [11]. Schematics of the discrete multiple V-shape ribs in air flow channel and range of potential parameters are shown in Tables 1 and 2, respectively. Developed correlations for Nu_{dmVr} and f_{dmVr} are also presented in Table 1. Authors found that by using this geometry the Nu_{dmVr} and f_{dmVr} can be increased by 6.74 and 6.37 times from smooth plate solar air channel, respectively.

3 Effect of Potential Parameters

The turbulent geometries that have been studied in the solar air channels can be standardized by defining the various geometrical parameters. In this section, these potential parameters associated with arc, discrete arc, multiple arc, discrete multiple arc, V-shape, discrete V-shape, multiple V-shape, and discrete multiple V-shape ribs along with their effect on the performance of solar air channel have been discussed.

3.1 Relative Roughness Pitch (P/e)

The relative roughness pitch is the ratio of pitch of ribs over the absorber plate to that of the height of the ribs. For ribs made up of circular wire, its thickness is equal to its height. From the previous studies, this has been found that the heat transfer rate upsurges with increase in P/e up to certain limit (generally 8–10) and afterward it decreases. The flow gets deviated toward the absorber plate as the fluid flow past a rib and resultingly flow reattachment points are created. Over these reattachment points, the heat transfer rate is maximum. As the fluid approaches toward the downstream rib, the boundary layer gets developed which results in lower convective heat transfer. So, the heat transfer rate decreases with the further increase in the P/e .

3.2 *Relative Roughness Height (e/D_h)*

The relative roughness height is expressed as the ratio of the rib height to that of the height of the rectangular channel. The relative roughness height affects the heat transfer enhancement in a duct flow of solar air heater. It is found that the heat transfer increases with increasing the relative roughness height. As the e/D_h increases, the turbulence due to more protrusions in flow increases. Because of this turbulence, the shear layer got reattached from the heated surface and the contact of main fluid stream occurred with the hot surface which result in heat transfer enhancement.

3.3 *Relative Angle of Attack ($A/90$)*

Relative angle of attack is the ratio of angle of attack to the right angle. Heat transfer rate is varied as the value of $\alpha/90$ is varied. The heat transfer rate firstly increases with increase in $\alpha/90$ and afterward decreases. Corresponding to 0.666 value of $\alpha/90$ from the centerline, the heat transfer rate has found maximum (0.333 from the edge). The arc and V-shape rib act as transverse ribs at larger values of $\alpha/90$ so significant heat transfer increment observed [13]. As the value of $\alpha/90$ decreases, the secondary fluid stream formation diminishes and results in comparatively less heat transfer augmentation.

3.4 *Relative Gap Position (D/x)*

Relative gap position (d/x) is the ratio of discrete distance from the leading edge of rib to the length of single limb. Heat transfer enhancement is greatly affected by variation in d/x . When the gap is placed near the trailing edge, the secondary flow contributes much in energizing the main flow and heat transfer rate increases resultingly. This effect of heat transfer augmentation diminishes as the discrete slice moves too near the apex. The maximum heat transfer is observed for $d/x \times 0.65-0.69$ but beyond this point the fluid mixing becomes again insignificant due to the increased length of the rib which results in truncation of secondary flow contribution in heat transfer.

3.5 *Relative Gap Width (g/e)*

The ratio of gap width to the height or thickness of the rib is called relative gap width (g/e). A significant effect of variation in g/e has been seen over the heat transfer. The heat transfer rate firstly increases with the increase in g/e until it attains value 1.0 and afterward starts decreasing. The secondary fluid stream gets developed along

the length of the rib and escape from the gap in the rib which results in energizing the main fluid stream and thereby heat transfer rate increases. The two contrasting effects of each other which govern the energy of secondary fluid stream passing through the discrete slice are the area of discrete slice and the tangential velocity of secondary stream. As the discrete area increases, the tangential velocity decreases and vice versa. So, because of this the average value of g/e attains maximum heat transfer and decreases at higher and lower values.

3.6 Relative Roughness Width (W/w)

Relative roughness width is the ratio of the roughness width to the single arc or V-shape rib width. The W/w affects the heat transfer and friction factor enhancement in duct flow of solar air channel. It is found that the performance of the solar air channel increases with increase in W/w up to certain limit (generally 5–6) and afterward starts decreasing. The reason for this trend could be as the roughness in form of arcs and Vs increases in the channel, and the secondary flow formation on the upstream side of the rib increases and thereby heat transfer rate also increases. As the number of arcs and Vs increase beyond a certain limit, the secondary flow streams increases but due to flow over a very small rib region their energy level decreases. So heat transfer rate decreases after this limit of W/w and friction factor increases.

4 Thermal and Friction Characteristics

Nusselt number and friction factor for different arrangements of ribs have been reproduced at varying values of Re by using the correlations provided in the literature. The prime values of the potential parameters suggested by the authors for different parameters of the geometries have been selected as standard of comparison. The obtained results are much close to the real experimental results of different geometries. Nusselt number for selected arrangement of ribs is presented in Fig. 1.

It can be clearly seen from Fig. 1 that the Nusselt number which signifies the heat transfer, increase with increase in flow rate, i.e., Re for all the selected rib geometries. The discrete V-shape ribs yields maximum Nusselt number from rest of the selected geometries at almost every value of Reynolds number in the chosen range. Multiple V-shape ribs and discrete multiple V-shape ribs shows quite high increment from other geometries. Similarly, values of friction factor for selected geometries have also been computed and presented in Fig. 2 w.r.t. Re .

Figure 2 shows the variation of friction factor with respect to the Re . The graph depicts that the friction factor decreases at higher flow rates. It can be clearly seen that the maximum hurdles to the flow to happen, i.e., maximum friction factor are offered by discrete multiple V-shape ribs while arc shape ribs offers least within the selected flow range, i.e., Re . The friction factor for all the geometries follows almost

Fig. 1 Variation of Nu with Re for different turbulent geometries

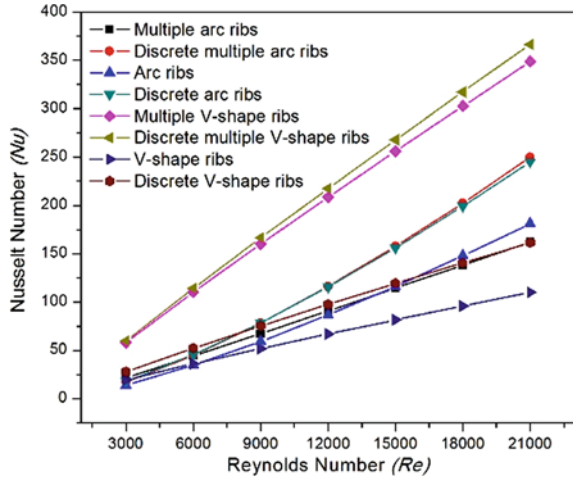
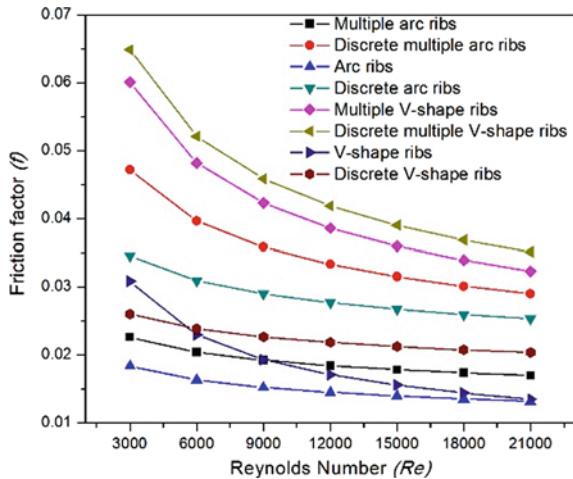


Fig. 2 Variation of friction factor with Reynolds number for different geometries



same trend of decreasing with Re due to destruction of laminar boundary layer at high flow velocities.

5 Performance Parameter

The performance parameters are standard of comparison for performance evaluation of different geometries of turbulators. In this section these parameters have been discussed for selected geometries.

5.1 Friction Factor and Thermal Enhancement

In contrast to smooth duct, the performances of different turbulent geometries have been obtained in terms of Heat transfer enhancement (HTE) and Friction factor enhancement (FFE). Mathematically,

$$HTE = Nu/Nu_s \tag{1}$$

$$FFE = f/f_s \tag{2}$$

Values of Nu_s and f_s has been computed by Dittus-Boelter and Blasius equations respectively. These equations are [12],

$$Nu_s = 0.023 \times Re^{0.8} \times Pr^{0.4} \tag{3}$$

$$f_s = 0.085 \times Re^{-0.25} \tag{4}$$

Results of the HTE and FFE for different Re have been presented in Fig. 3.

The graphs shows that HTE is maximum for discrete multiple V-shape ribs and minimum for upward V-shape ribs. FFE is also found maximum for discrete multiple V-shape ribs and minimum for arc ribs. In order to attain maximum performance HTE should be at highest possible value and FFE should be at least.

Fig. 3 HTE and FFE for different geometries at variable values of Reynolds number

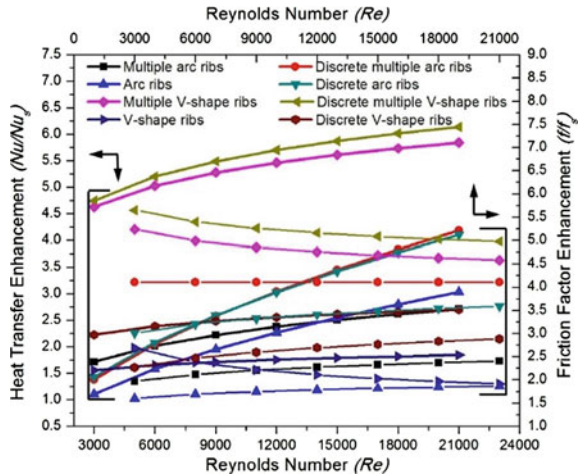
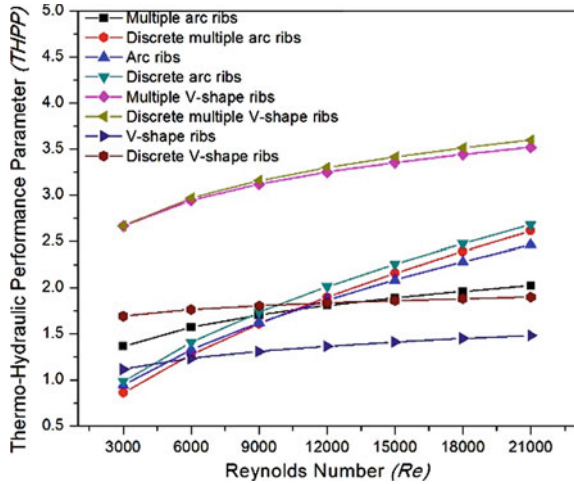


Fig. 4 THPP for different arrangements of ribs



5.2 Thermo-Hydraulic Performance Parameter (THPP)

The combined effect of HTE and FFE can be studied by computing the thermo-hydraulic performance parameter (THPP). Mathematically, THPP is given as [11],

$$THPP = HTE / (FFE)^{1/3} \tag{5}$$

The results of THPP for different arrangements of ribs have been presented in Fig. 4.

Figure 4 shows that the THPP is maximum for discrete multiple V-shape ribs and is followed by multiple V-shape ribs. The minute difference between THPP of these leading two roughness geometries can be seen only at high values of Re but for low flow rates both these performs almost equally. For Re below 6000, THPP is 1% more and for Re between 6000 and 21,000 THPP is 2% more for discrete multiple V-shape ribs than multiple V-shape ribs.

6 Conclusion

This study has been conceded to find the most appropriate arrangement of ribs in shape of arc and V-shape, placed in single-pass solar air channel which can offer maximum heat transfer rate at minimum expense of friction factor. The broad conclusions of this study are,

- Nusselt number and friction factor have been estimated by using correlations provided in literature for Re range of 3000–21,000. The top three geometries that

performs best in terms of Nusselt number and friction factor are, discrete multiple V-shape ribs > multiple V-shape ribs > discrete multiple arc ribs.

- Heat transfer enhancement (HTE) and friction factor enhancement (FFE) have been computed for selected geometries of ribs and found maximum HTE of 6.13 at Reynolds number 21000 and FFE of 5.64 at Reynolds number 3000 for discrete multiple V-shape ribs.
- Thermo-hydraulic performance parameter (THPP) has been calculated and top two turbulent geometries which facilitates maximum THPP are discrete multiple V-shape ribs and multiple V-shape ribs.
- THPP is minutely additional for discrete multiple V-shape ribs from multiple V-shape ribs of 1% for $Re < 6000$ and 2% for $6000 < Re < 21,000$. So any of these geometries can be used according to need of application.

This study can be useful for identifying most appropriate arrangement of ribs at different values of Reynolds number. Further studies can be carried out to compare other turbulent geometries to found optimum one for different flow conditions according to demand of applications.

References

1. Sharma, A., Chauhan, R., Singh, T., Kumar, A., Kumar, R., Kumar, A., & Sethi, M. (2017). *Renewable Energy*, 106, 310–320.
2. Prasad, B. N., & Saini, J. S. (1988). *Solar Energy*, 41, 555–560.
3. Kumar, A., & Layek, A. (2019). *Renewable Energy*, 130, 687–699.
4. Saini, S. K., & Saini, R. P. (2008). *Solar Energy*, 82, 1118–1130.
5. Hans, V. S., Gill, R. S., & Singh, S. (2017). *Experimental Thermal and Fluid Science*, 80, 77–89.
6. Singh, A. P., Varun & Siddhartha (2014). *Experimental Thermal and Fluid Science*, 54, 117–126.
7. Pandey, N. K., & Bajpai, V. K. (2016). *Solar Energy*, 134, 314–326.
8. Momin, A. M. E., Saini, J. S., & Solanki, S. C. (2002). *International Journal of Heat and Mass Transfer*, 45, 3383–3396.
9. Singh, S., Chander, S., & Saini, J. S. (2011). *Energy*, 36, 5053–5064.
10. Hans, V. S., Saini, R. P., & Saini, J. S. (2010). *Solar Energy*, 84, 898–911.
11. Kumar, A., Saini, R. P., & Saini, J. S. (2013). *Renewable Energy*, 58, 151–163.
12. Singh, I., & Singh, S. (2018). *Renewable and Sustainable Energy Reviews*, 92, 405–425.
13. Kumar, R., Chauhan, R., Sethi, M., Sharma, A., & Kumar, A. (2016). *Advances in Mechanical Engineering*, 8, 1–12.